

Evaluation of performances of solid oxide fuel cells with symmetrical electrode material

Peng Zhang ^a, Guoqing Guan ^{a,b,*}, Deni S. Khaerudini ^a, Xiaogang Hao ^c, Chunfeng Xue ^c, Minfang Han ^d, Yutaka Kasai ^e, Abuliti Abudula ^{a,b,*}

^a Graduate School of Science and Technology, Hirosaki University, 1-bunkyocho, Hirosaki 036-8560, Japan

^b North Japan Research Institute for Sustainable Energy (NJRSE), Hirosaki University, 2-1-3 Matsubara, Aomori 030-0813, Japan

^c Department of Chemical Engineering, Taiyuan University of Technology, Taiyuan 030024, China

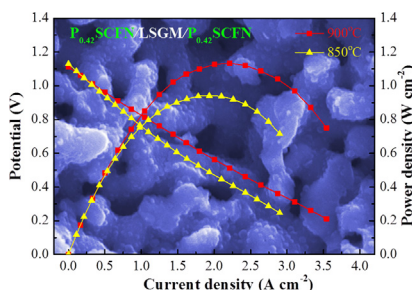
^d Union Research Center of Fuel Cell, School of Chemical & Environmental Engineering, China University of Mining & Technology, Beijing 100083, PR China

^e Industrial Research Institute, Aomori Prefectural Industrial Technology Research Center, 4-11-6, Second Tonyamachi, Aomori 030-0113, Japan

HIGHLIGHTS

- P_xSCFN oxide is developed as symmetrical electrode material for SOFC.
- Pr element content in P_xSCFN has great effect on SOFC performance.
- Nano-sized Co-enriched particles are obviously formed in anode side.
- Pr^{3+}/Pr^{4+} , Co^{2+}/Co^{3+} and $Fe^{2+}/Fe^{3+}/Fe^{4+}$ coexist in P_xSCFN .

GRAPHICAL ABSTRACT



ARTICLE INFO

Article history:

Received 6 February 2014

Received in revised form

9 April 2014

Accepted 5 May 2014

Available online 13 May 2014

Keywords:

Solid oxide fuel cells

P_xSCFN

XPS

Nano-size Co-enriched

A-site excess

Symmetrical electrode

ABSTRACT

$Pr_xSr_{0.6}Co_{0.2}Fe_{0.7}Nb_{0.1}O_{3-\sigma}$ (P_xSCFN , $x = 0.38, 0.40, 0.42$ and 0.44) oxide has been developed as symmetrical electrode material for solid oxide fuel cell (SOFC) in our group. In this study, the effect of Pr element contents on the cell performance of the P_xSCFN symmetrical electrode SOFC is investigated in details. Electrochemical impedance spectra (EIS) technique, scanning electron microscopy (SEM), and energy dispersive X-ray spectroscopy (EDX) are used to characterize the electrodes after the performance test. It is found that the nano-sized Co-enriched particles are obviously formed in anode side, which could contribute to the high catalytic activity of the P_xSCFN symmetrical electrode materials. An optimum x value, i.e., 0.42, is found for the P_xSCFN symmetrical electrode materials. As-prepared single cell shows an average slow degradation rate of 0.5 mV h^{-1} during 100 h stability test, indicating that the symmetrical SOFC with $PSCFN$ as electrode has the acceptable stabilization. X-ray photoelectron spectroscopy (XPS) analysis indicated that the content of Si^{2+} species on the surface decreases to some extent in the case of A-site Pr element slight excess, which could result in the promoting of the catalytic properties of $PSCFN$ material.

© 2014 Elsevier B.V. All rights reserved.

1. Introduction

Solid oxide fuel cells (SOFCs) are electrochemical devices that have advantages of high efficiency, low pollution, fuel flexibility and long term stability and other features which make them attractive for energy conversion [1,2]. Hydrogen is considered the

* Corresponding authors. Graduate School of Science and Technology, Hirosaki University, 1-bunkyocho, Hirosaki 036-8560, Japan. Tel.: +81 17 762 7756; fax: +81 17 735 5411.

E-mail addresses: guan@cc.hirosaki-u.ac.jp (G. Guan), abuliti@cc.hirosaki-u.ac.jp (A. Abudula).



best fuel for SOFC, but the issues related to its generation, storage and transportation still hinder its large-scale utilization in SOFC. Instead, hydrocarbon fuels become good alternatives for the commercial utilization of SOFC [3]. To date, Ni-YSZ is a widely-used anode material in SOFC; however, hydrocarbon fuels are easy to be catalytically cracked on Ni, leading to carbon deposited on the surface of the anode and decrease the cell performance. On the other hand, sulfur, even at the magnitude of part per million (ppm) levels in the fuel, could be adsorbed on Ni sites and block its activity for the catalytic oxidation of fuel [4]. In order to solve these problems, Symmetrical electrode SOFC, in which the same material is used in both anode and cathode, was proposed [4–6]. In such symmetrical electrode SOFCs, the possible coke formation and/or sulfur poisoning on the surface of the anode can be potentially eliminated and thereby the anode is regenerated by operating the anode as the cathode in turn; where carbon or sulfur species absorbed on the electrode could be burnt out by oxidant. Simultaneously, the durability of cathode could also be improved in the low O₂ partial pressure at triple phase boundary region of cathode side [5]. In addition, the process for the preparation of the cell becomes more easily since the electrodes may be fired using the same thermal process. This would significantly save fabrication time and reduce the cost.

It is a key issue to develop a symmetrical electrode material with high catalytic activity for commercial utilization of such SOFCs, especially for those SOFCs work in hydrocarbon fuels containing H₂S. Bastidas et al. [4] considered La_{0.75}Sr_{0.25}Cr_{0.5}Mn_{0.5}O₃ (LSCM) as the symmetrical electrode material, and found that the prepared LSCM/YSZ/LSCM cell showed the maximum power density of 0.3 W cm⁻² at 900 °C. Ruiz-Morales et al. [5] optimized microstructure of LSCM and achieved a maximum power density of 0.5 W cm⁻² at 950 °C by using wet H₂ as fuel. Zhu et al. [6] added Sm-doped CeO₂ (SDC) or Ni into LSCM symmetrical electrode and found that addition of 6 wt.% Ni to the anode resulted in the highest power density value reached 0.559 W cm⁻² at 900 °C, which was better than those cells with the addition of SDC. Liu et al. [7] used Sr₂Fe_{1.5}Mo_{0.5}O₆ – σ (SFM) as the symmetrical electrode material, and the obtained SFM/LSGM/SFM symmetrical cell reached the maximum power densities of 0.835 and 0.23 W cm⁻² at 900 °C in wet H₂ and CH₄, respectively. They investigated the redox stability upon a 5 redox cycle test at 800 °C, and found that there was no any adverse effect on the maximum power output after 5 redox cycles. However, the cell performance was lower than the conventional Ni-based SOFC. Martinez-Coronado et al. [8] used La_{0.5}Sr_{0.5}Co_{0.5}Ti_{0.5}O₃ – σ (LSCT) as the symmetrical electrode material, and obtained a maximum power density of 0.11 W cm⁻². Chen et al. [9] used Sr-rich La_{0.3}Sr_{0.7}Fe_{1 – x}Cr_xO₃ – σ (LSFC_x, x = 0–0.3) as the symmetrical electrode material, and obtained the maximum power density of 0.3 W cm⁻² at 800 °C in wet H₂ for LSFC_{0.3} sample. All these reported symmetrical electrode material showed relatively low power density performance.

In our previous study [10], Pr_xSr_{0.6}Co_{0.2}Fe_{0.7}Nb_{0.1}O₃ – σ (P_xSCFN, x = 0.38–0.44) was synthesized and used as the symmetrical electrode. It is found that the excess of A-site Pr element in P_xSCFN, i.e., in the cases of x = 0.42 and 0.44, resulted in a decrease in grain size and the creation of more active sites for oxygen reduction reaction. AC impedance measurements revealed that P_{0.42}SCFN had the best electrochemical catalytic performance in both O₂ and wet H₂ atmospheres. The maximum power densities of the prepared P_{0.42}SCFN/LSGM/P_{0.42}SCFN cell reached as high as 1.13 W cm⁻² in wet H₂ and 0.67 W cm⁻² in wet CH₄ at 900 °C. In this study, the effect of Pr element contents on the cell performances of the P_xSCFN (x = 0.38, 0.40, 0.42 and 0.44) symmetrical electrode SOFC were investigated in more details. Electrochemical impedance

spectra (EIS) technique, scanning electron microscopy (SEM), and energy dispersive X-ray spectroscopy (EDX) were used to characterize the electrodes after the performance test. Furthermore, in order to understand the promoting catalytic properties of P_xSCFN materials, X-ray photoelectron spectroscopy (XPS) analysis was used to investigate the existence states of Pr³⁺/Pr⁴⁺, Co²⁺/Co³⁺, Fe²⁺/Fe³⁺/Fe⁴⁺ and Sr²⁺ species in the PSCFN sample. The obtained results were analyzed and discussed in details.

2. Experimental

2.1. Sample preparation and cell fabrication

P_xSCFN (x = 0.38, 0.40, 0.42 and 0.44) perovskite oxides were prepared by solid-state reaction from the chemicals with high purity: Pr(NO₃)₃·6H₂O, SrCO₃, Co(NO₃)₂·6H₂O, Fe₂O₃ and Nb₂O₅ (99.9% Wako, Japan) [10]. Commercially available powder, La_{0.8}Sr_{0.2}Ga_{0.8}Mg_{0.2}O₃ – σ (LSGM, 99.9% FCM, USA) was used for the preparation of electrolyte. Dense LSGM pellets with 20 mm in diameter were prepared by uniaxial mold pressing LSGM powder at 200 MPa and then sintering at 1450 °C for 10 h in air. After sintering, the electrolyte disk was approximately 20.0 mm in diameter and around 0.265 mm in thickness.

Symmetrical electrode cells of P_xSCFN/LSGM/P_xSCFN for the impedance study were prepared by slurry coating method. That was, P_xSCFN slurry was coated onto both sides of LSGM electrolyte pellet to form the anode and cathode and then, as-prepared cell was sintered in air at 1200 °C for 2 h. The effective area of porous electrode was about 0.38 cm² with a thickness of about 30 μm. For a single cell performance testing, the cell was sealed on an alumina tube using a Pyrex glass ring. Such measurements were carried out in a temperature range of 750–900 °C. For the single cell performance test, the anode was first annealed at 900 °C in pure H₂ atmosphere for 1 h, and then exposed to fuel at a flow rate of 100 cm³ min⁻¹. O₂ was used in the cathode side as the oxidant with a flow rate of 50 cm³ min⁻¹. Electronic contacts were realized by using a Pt mesh with Pt paste. It is reported that Pt has almost no influence on the electrode catalytic activity [11–14]. Electrochemical impedance spectra (EIS) of the single cell after the cell performance test were recorded at open circuit voltage (OCV) over the frequency range of 0.1 Hz–1 MHz with the AC signal amplitude of 10 mV using a frequency response analyzer and a potentiostat (Solartron 1255B and 1287, respectively). The impedance responses were analyzed using the equivalent RC circuit method.

2.2. Material characterization

Morphology and element composition were investigated by scanning electron microscopy (SEM, Hitachi, SU6600, Japan) with an EDX detector. Surface composition and valence of each element were identified for fresh powders by X-ray photoelectron spectroscopy (XPS, AXIS ULTRA DLD, Japan). A monochromatic Al K α source ($h\nu$ = 1486.6 eV) was used at a power of 150 W. Binding energy were calibrated with respect to setting the measured binding energy of C1s at 248.8 eV. Resolution of all spectra was performed by XPS Peak Program (XPSPEAK 4.1).

3. Results and discussion

3.1. Cell performance analysis

Current–potential (I–V) characteristics of LSGM electrolyte supported symmetrical electrode SOFCs with P_{0.38}SCFN, P_{0.40}SCFN, P_{0.42}SCFN and P_{0.44}SCFN as the electrode are shown in Fig. 1. The

performances of cells were tested at different temperatures (750–900 °C) with wet hydrogen as fuel and oxygen as oxidant. One can see that the power density increased with the increase in the operating temperature for all single cells. Open-circuit voltage (OCV) of all cells was approximately 1.1 V at 900 °C and increased with the decreasing of temperature. The maximum power densities of 0.653, 0.859, 1.133 and 0.972 W cm⁻² at 900 °C were achieved for the cells using P_{0.38}SCFN, P_{0.40}SCFN, P_{0.42}SCFN and P_{0.44}SCFN as the symmetrical electrode, respectively. It should be noted that the performances of these single cells were much higher than those reported symmetrical electrode SOFCs by other research groups as introduced above [4,5,11–13], indicating that P_xSCFN material is suitable for the symmetrical electrode SOFC with a high performance.

The performance of the cells with P_xSCFN ($x = 0.38, 0.40, 0.42$ and 0.44) symmetrical electrode was improved by increasing Pr element content when $x \leq 0.42$; however, when further increased x to 0.44, the power density slightly decreased at each temperature. As $x = 0.42$, the maximum power density reached 0.941, 0.762 and 0.578 W cm⁻² at 850, 800 and 750 °C, respectively; However, as $x = 0.44$, these values decreased to 0.801, 0.645 and 0.485 W cm⁻², respectively. In our previous study [10], it is found that there was impurity phase in the sample as $x = 0.44$, may causing the decline of cell performance. As indicated in Fig. 1 (a), (b) and (c), the cell performance increased more obviously for higher Pr element contents by elevating the operation temperature. One can see that P_{max} increased from 0.488 to 0.653 W cm⁻² as $x = 0.38$ and 0.578–1.133 W cm⁻² as $x = 0.42$ by increasing temperature from 750 to 900 °C. It indicated that the power density for P_{0.42}SCFN based cell increased 96% by increasing temperature, which is much higher than the increase extent (33.8%) for P_{0.38}SCFN based cell.

3.2. Electrochemical impedance spectra

Electrochemical impedance spectra of the single cells with P_xSCFN ($x = 0.38, 0.40, 0.42$ and 0.44) symmetrical electrodes

under open circuit conditions between 750 and 900 °C are given in Fig. 2. Herein, the highest frequency intercept on the real axis represents the overall ohmic resistance (R_{ohm}) from the electrolyte, the electrodes, interfaces between electrolyte and electrodes under the testing conditions [15]. The lowest frequency intercept on the real axis represents the total resistance (R_{total}) of the cell. The distance between the two intercepts corresponds to polarization resistance (R_p) [16], which mainly corresponds to the adsorption and diffusion processes of oxygen on the cathode and hydrogen on the anode. As shown in Fig. 2, both R_{ohm} and R_p decreased by increasing temperature from 750 to 900 °C for all cells. For instances, in Fig. 2(c) where $x = 0.42$, R_{ohm} values were 0.28, 0.24, 0.21 and 0.20 Ω cm² at 750, 800, 850 and 900 °C, respectively while R_p values were about 0.53, 0.36, 0.24 and 0.17 Ω cm² at 750, 800, 850 and 900 °C, respectively.

To compare the impedance data of different cells with different P_xSCFN ($x = 0.38, 0.40, 0.42$ and 0.44) symmetrical electrodes, the fitted impedance results for single P_xSCFN symmetrical cells are given in Fig. 3, in which the effect of A-site Pr element contents on R_{total}, R_{ohm} and R_p at 900 °C was indicated. One can see that R_{ohm} decreased by increasing x value from 0.38 to 0.42; however, by further increasing x value to 0.44, R_{ohm} increased to some extent. It should be noted that all cells had almost the same electrolyte thickness and were tested in the same conditions in this study. Thus, the difference of R_{ohm} should mainly be resulted from the differences of electrode materials and the interfacial resistances between electrolyte and electrodes. However, as indicated in our previous study [10], the electrical conductivity of all the P_xSCFN samples are similar at the temperature range from 750 to 900 °C. Therefore, the decrease of R_{ohm} of P_xSCFN symmetrical electrode cell should be attributed to the interfacial resistance between LSMG electrolyte and P_xSCFN electrodes. From Fig. 3, the R_{total} values of the cells were 0.51, 0.41, 0.37 and 0.43 Ω cm² at 900 °C for $x = 0.38, 0.40, 0.42$ and 0.44 , respectively. The lowest total resistance of 0.37 Ω cm² was also achieved as $x = 0.42$, which is consistent with the cell performances. Herein, the lower interfacial resistance of

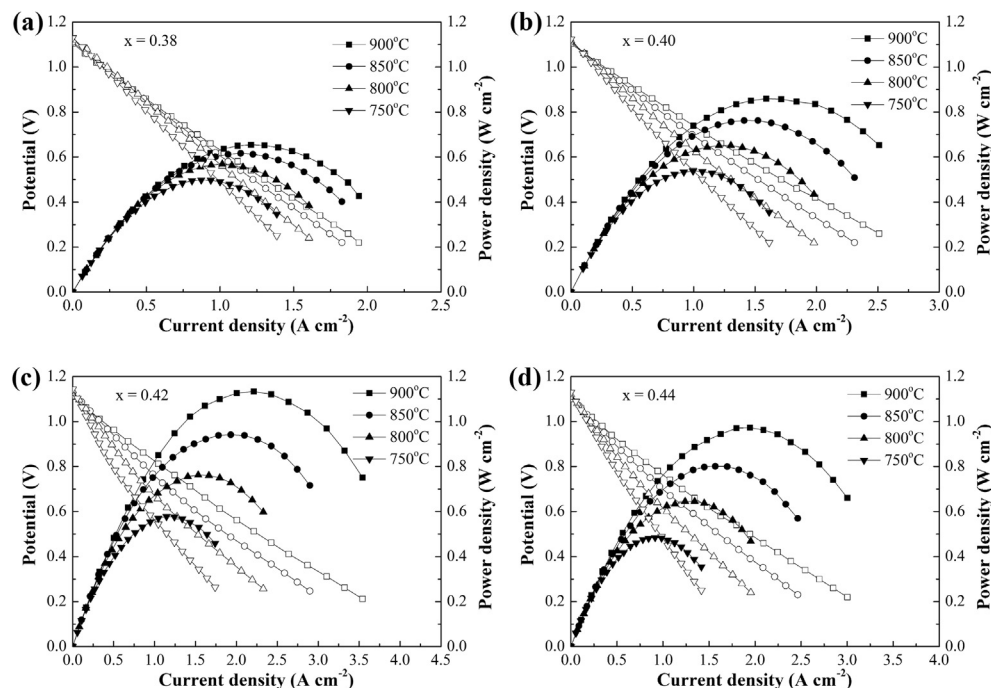


Fig. 1. I–V curves and corresponding power density curves of the single cells (P_xSCFN/LSGM/P_xSCFN) under various temperatures: (a) $x = 0.38$, (b) $x = 0.40$, (c) $x = 0.42$ and (d) $x = 0.44$.

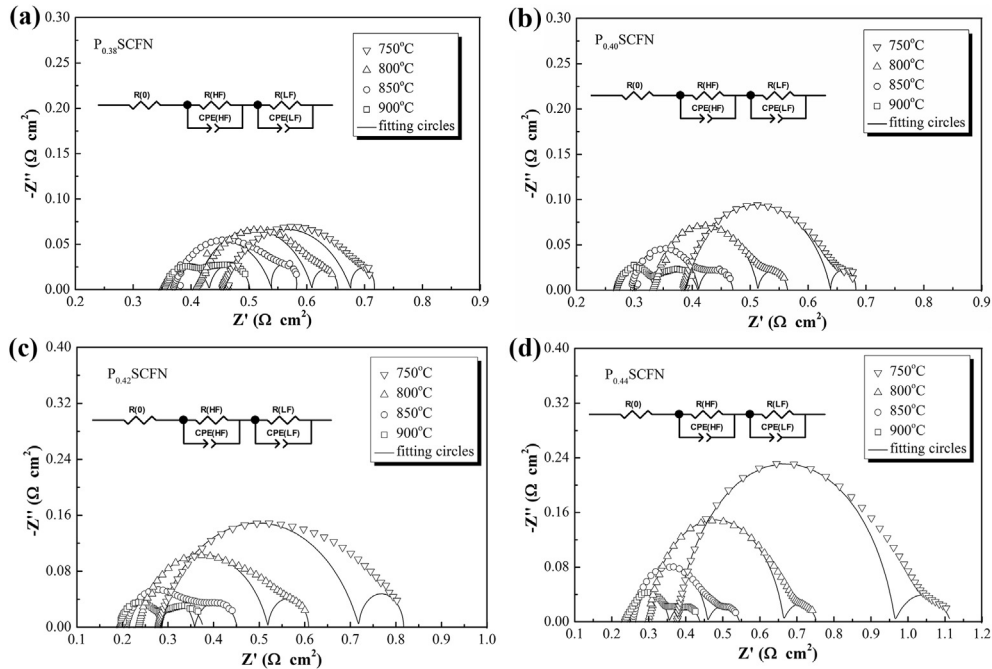


Fig. 2. Impedance spectra of the single cells ($P_x\text{SCFN}/\text{LSGM}/P_x\text{SCFN}$) measured under OCV using H_2 as a fuel and O_2 as an oxidant at various temperatures: (a) $x = 0.38$, (b) $x = 0.40$, (c) $x = 0.42$ and (d) $x = 0.44$. The solid lines are the fitted curves, and the equivalent circuit used for fitting the impedance data are also shown.

$P_{0.42}\text{SCFN}$ symmetrical electrode cell than others should be due to the good contact between the $P_{0.42}\text{SCFN}$ electrode and LSGM electrolyte, which will be further discussed in the section 3.3.

3.3. SEM images

Fig. 4 shows the cross-sectional SEM images of the single cell (PSCFN/LSGM/PSCFN) after the performance test. It clearly shows the sandwich structures of the whole cell, where the thickness of cathode, electrolyte and anode were approximately 30, 265 and 30 μm , respectively. No micro-cracks or delamination were observed in the SEM image.

The cross section images of interface between $P_x\text{SCFN}$ anode and LSGM electrolyte after cell performance test were shown in Fig. 5. From Fig. 5, one can see that the grain size of $P_x\text{SCFN}$ electrodes

decreased by increasing x value from 0.38 to 0.42 and similar grain size was observed as $x = 0.44$ and 0.42. Zhou et al. [17] and Jaffe et al. [18] also found that the grain size decreased by making A-site a slight excess. The decrease of grain size could result in larger three phase boundary (TPB) and provide larger reaction area. This may be the main reason why the cell performance of $P_{0.42}\text{SCFN}$ was better than those of $P_{0.38}\text{SCFN}$ and $P_{0.40}\text{SCFN}$ symmetrical electrode cells. Sumi et al. [19] believed that the grain size on the electrodes had great effect on the length of phase boundaries, the electronic conduction paths and the contact areas between the electrode and electrolyte. For the present $P_{0.42}\text{SCFN}$ symmetrical electrode, the smaller grain size could decrease the contact resistance between the electrode and electrolyte due to larger contact areas with the LSGM electrolyte when compared with $P_{0.40}\text{SCNF}$ and $P_{0.38}\text{SCFN}$.

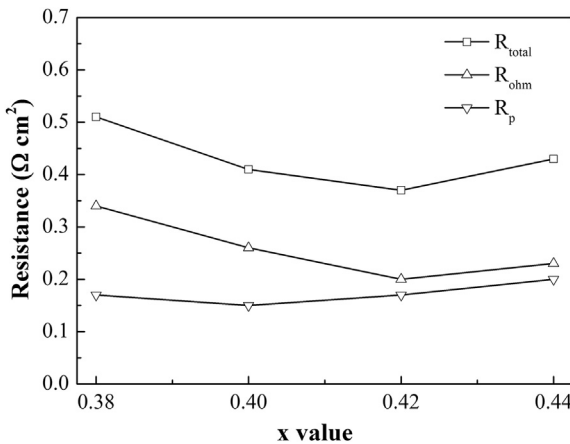


Fig. 3. Dependence of the R_{ohm} , R_p and R_{total} for the single cell ($P_x\text{SCFN}/\text{LSGM}/P_x\text{SCFN}$) with different Pr element contents at 900 °C using H_2 as a fuel and O_2 as an oxidant at 900 °C.

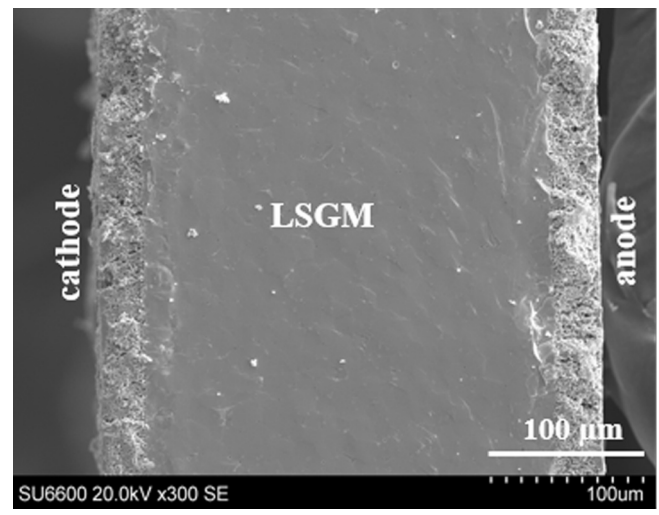


Fig. 4. Cross-sectional SEM image of the single cell PSCFN/LSGM/PSCFN after performance test.

based cells. This may also be the main reason why the lowest R_{ohm} value was obtained for $P_{0.42}\text{SCFN}$ symmetrical electrode SOFC, as indicated in section 3.2. On the other hand, for $P_{0.44}\text{SCFN}$ symmetrical electrode, although its grain size was similar as the $P_{0.42}\text{SCFN}$ sample, the cell performance decreased to some extent, which may be caused by the impurity phase in $P_{0.44}\text{SCFN}$ according to XRD patterns in our previous study [10].

From the cross section images of the cathode side after the cell performance test, as shown in Fig. 6(a) and (b), fine uniform microstructure can be found; however, for the anode side, as shown in Fig. 6(c) and (d), some small particles, which were proved to be nano-sized Co-enriched particles by EDX, as shown in Fig. 7, were found to be dispersed on the surface of the grain. Such dispersed particles could serve as the catalyst for the reactions happened in anode side [20]. Scurtu et al. [21] also observed such Co-enriched phenomenon on the surface of perovskite oxides. It is reported that Co element had higher catalytic activity for oxidant reactions than Fe, and Co was also enriched on the surface of other electrodes after performance test [22,23]. Pan et al. [24] calculated the binding energy values of Fe–O and Co–O bonds, and found that the binding energy of Co–O was lower than Fe–O. That may be the main reason why Co is easily enriched on the surface of the anode. From Fig. 6(c) and (d), the amount of Co-enriched particles of $P_{0.42}\text{SCFN}$ sample was more than that on the $P_{0.40}\text{SCFN}$ anode surface, which may contribute to the higher catalytic activity of $P_{0.42}\text{SCFN}$ anode.

3.4. Stability test

100 h stability test was performed with $P_{0.42}\text{SCFN}$ as symmetrical electrode for a single cell: $P_{0.42}\text{SCFN}/\text{LSGM}/P_{0.42}\text{SCFN}$ with LSGM as the electrolyte supported layer. The surface areas of LSGM electrolyte and both electrodes are 3.14 and 0.38 cm^2 , respectively. The thickness of LSGM layer is about 275 μm . The test was performed at a constant current density of 0.93 A cm^{-2} at 800°C , with

$100 \text{ cm}^3 \text{ min}^{-1}$ wet H_2 (3% H_2O) flow at anode side and $50 \text{ cm}^3 \text{ min}^{-1}$ O_2 flow at cathode side. As shown in Fig. 8, an average slow degradation rate of 0.5 mV h^{-1} during 100 h stability test was found. It indicates that the symmetrical SOFC with $P_{0.42}\text{SCFN}$ as electrode has the acceptable stabilization during 100 h test.

3.5. XPS analysis

In order to understand the large difference of power density obtained by different $P_x\text{SCFN}$ ($x = 0.38, 0.40, 0.42$ and 0.44) based symmetrical electrode SOFC, the surface composition of the $P_x\text{SCFN}$ materials were also characterized using XPS technique. To describe the different features of the different $P_x\text{SCFN}$ samples, the Pr 3d, Sr 3d, Co 2p, Fe 2p and O 1s core-level XPS spectra were obtained. Fig. 9 illustrates the Pr 3d core-level XPS spectra of $P_{0.42}\text{SCFN}$ sample. A spin-orbit-splitting energy of 20.6 eV was found between the Pr $3d_{5/2}$ and Pr $3d_{3/2}$ lines. The intensity ratio between the two spin-orbit components is in agreement with the expected statistical ratio of 2/3. The Pr $3d_{5/2}$ spectra, at $\sim 933 \text{ eV}$, presented one main peak and one shoulder separated by a binding energy of 4.6 eV. The peaks that envelope the Pr^{3+} and Pr^{4+} oxidation states are fitted in Fig. 9. The main peaks at 927.9 and 932.9 eV are representative of Pr^{3+} $3d_{5/2}$, whereas the peaks at 931.0 and 935.2 eV can be assigned to Pr^{4+} $3d_{5/2}$ [25], indicating that the oxidation states of Pr in the compound are 3+ and 4+, which may contribute to the electrocatalytic properties. Ishihara et al. [26] reported that higher electrical conductivity and lower overpotential values resulted from the introduction of Pr element into $\text{Ln}_{0.6}\text{Sr}_{0.4}\text{MnO}_{3-\sigma}$ ($\text{Ln} = \text{La}, \text{Pr}, \text{Nd}, \text{Sm}, \text{Gd}, \text{Yb}$ and Y) should be due to the $\text{Pr}^{3+}/\text{Pr}^{4+}$ valence change. Jin et al. [27] also found that $\text{Pr}^{3+}/\text{Pr}^{4+}$ coexisted in the oxides of $\text{PrBaCo}_{2/3}\text{Fe}_{2/3}\text{Cu}_{2/3}\text{O}_{5+\sigma}$. Tsipis et al. [28] suggested that infiltration of Pr into electrode materials should be a suitable way to enhance the surface exchange kinetics and electrocatalytic activity. He et al. [29] and Yaremchenko et al. [30]

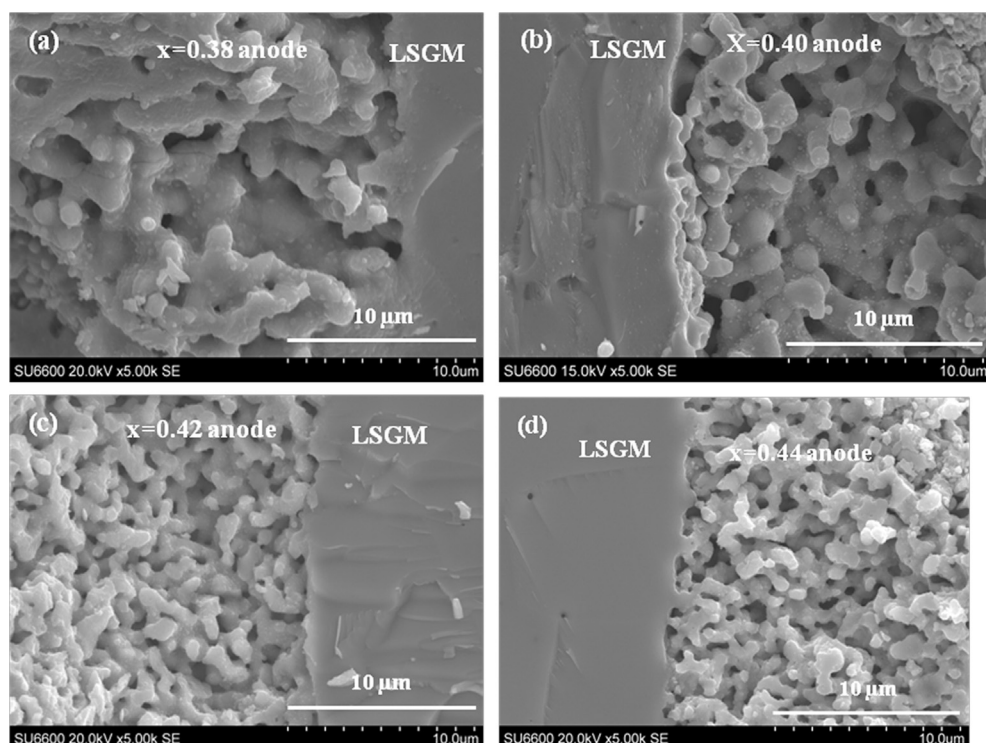


Fig. 5. SEM images of $P_x\text{SCFN}$ anode and LSGM electrolyte after cell performance test: (a) $x = 0.38$; (b) $x = 0.40$; (c) $x = 0.42$; (d) $x = 0.44$.

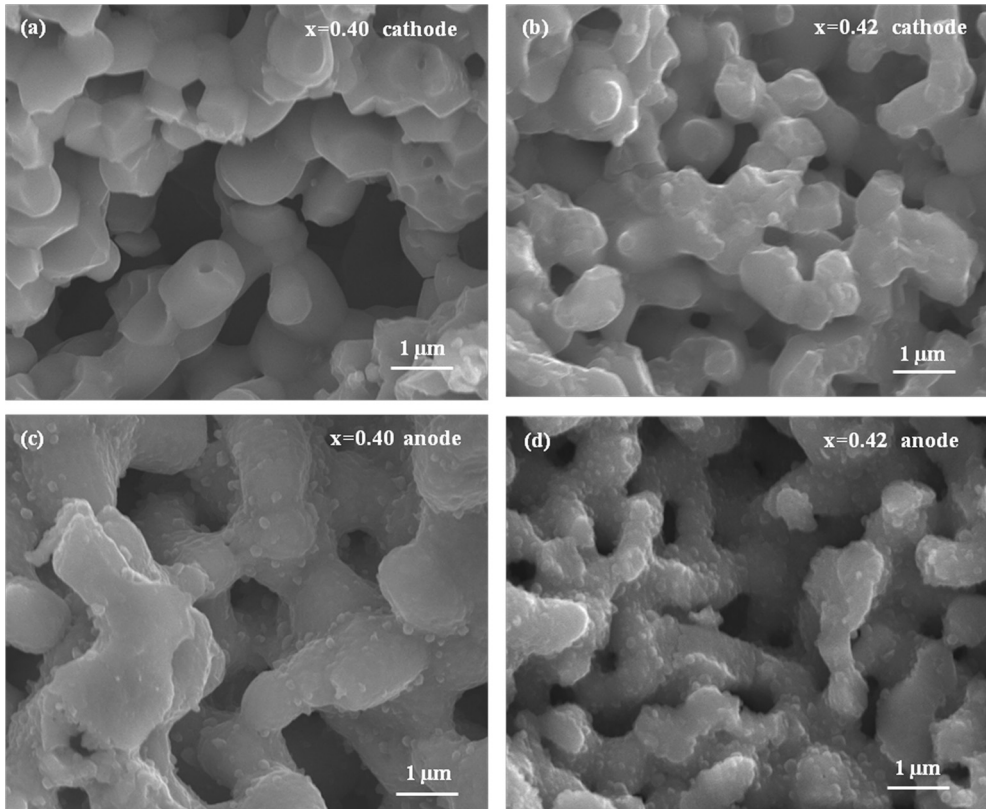


Fig. 6. Cross section images of: (a) $P_{0.40}$ SCFN cathode; (b) $P_{0.42}$ SCFN cathode; (c) $P_{0.40}$ SCFN anode and (d) $P_{0.42}$ SCFN anode after cell performance test.

also reported Pr had a mixed state of Pr^{3+} and Pr^{4+} in the electrode materials. For P_x SCFN samples, the ion state change between Pr^{3+} / Pr^{4+} could be promoted by increasing the Pr element content. As a result, an enhancement of the catalytic activity in the reaction related to the cell operation could be realized.

The Sr 3d core-level XPS spectrum of $P_{0.40}$ SCFN and $P_{0.42}$ SCFN are shown in Fig. 10. It is reported that Sr 3d band showed multiple components [31,32]. A careful fitting procedure allowed identifying

four components, namely two Sr 3d_{5/2} doublets with 1.79 eV splitting between 3d_{5/2} and 3d_{3/2} peaks, and it is found that the value is excellent agreement with literature data [31,33]. Herein, assignments were made on the basis of the angle-resolved studies. In Fig. 10(a), the Sr 3d_{5/2} contribution at 131.6 eV is assigned to Sr present within the bulk of these oxides such as SrO_{1-x} suboxide [22], thus this component can be assigned to Sr^{2+} ions surrounded by vacancies in the oxygen-deficient perovskite structure [31]. The

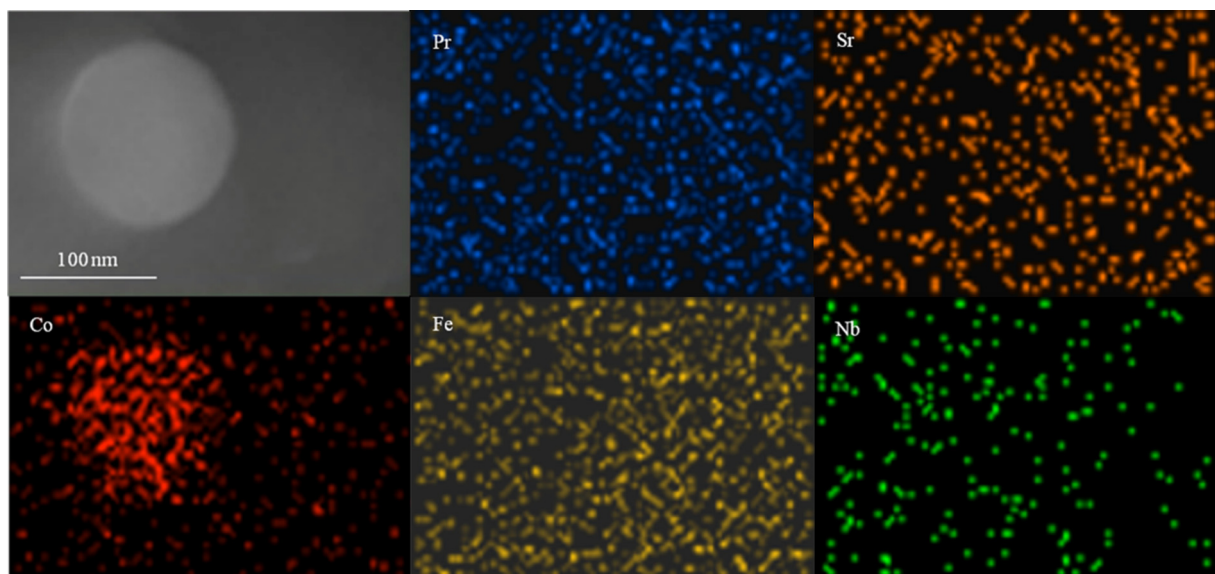


Fig. 7. Pr, Sr, Co, Fe and Nb mapping analysis of the nano-sized particle on the anode surface after cell performance test.

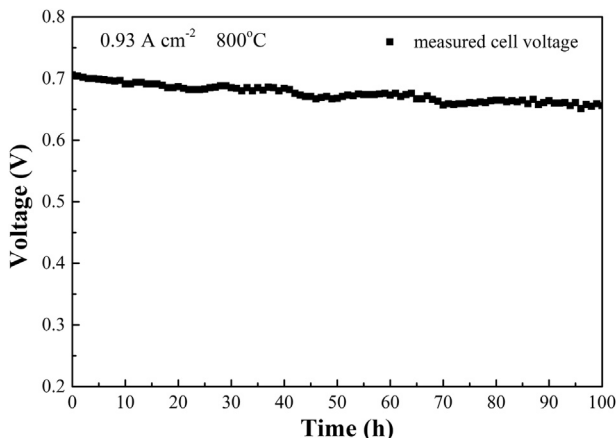


Fig. 8. Stability test of $P_{0.42}SCFN/LSGM/P_{0.42}SCFN$ symmetrical SOFC, measured at 800°C with wet H_2 as the fuel and O_2 as the oxidant.

peak at 133.0 eV is due to Sr appeared at the outermost surface, which can be attributed to SrCO_3 (~ 133.2 eV) [21]. The peak at high binding energy of 134.8 eV can be assigned to SrO present on the surface of the oxides, which also observed by others [34]. Comparing both XPS spectrum of $P_{0.40}SCFN$ and $P_{0.42}SCFN$ samples, the area at high binding energy as $x = 0.40$ is larger than that of $x = 0.42$ sample, indicating that the slight excess of A-site Pr element can decrease the surface of SrO , which could be benefit for the promotion of catalytic performance of materials [35]. Therefore, the better performance of $P_{0.42}SCFN$ than the no A-site excess sample of $P_{0.40}SCFN$ may be due to the decrease of surface SrO content.

The Co 2p core-level XPS spectra is normally a distorted peak, which results from complex state effects. As shown in Fig. 11(a), for $P_{0.42}SCFN$, the Co 2p XPS region showed a doublet, i.e., $2\text{p}_{3/2}$ and $2\text{p}_{1/2}$. The splitting energy of 15.2 eV was found between Co 2p_{3/2} and Co 2p_{1/2}. The peaks at 779.9 and 781.2 eV were assigned as Co^{3+} and Co^{2+} , respectively [36,37]. The presence of the satellite peaks at about 6.5 eV from the high energy component should be a further evidence for Co^{2+} species [37]. Harvey et al. [38] and Yang et al. [39] reported that Co^{2+} and Co^{3+} can transform between each other at temperatures higher than 800°C , and the presence of compounds of Co^{2+} and Co^{3+} suggested that Co is chemically active in perovskite structure. Therefore, the sharp improvement of cell performance of $P_{0.42}SCFN$ symmetrical electrode SOFC by elevating

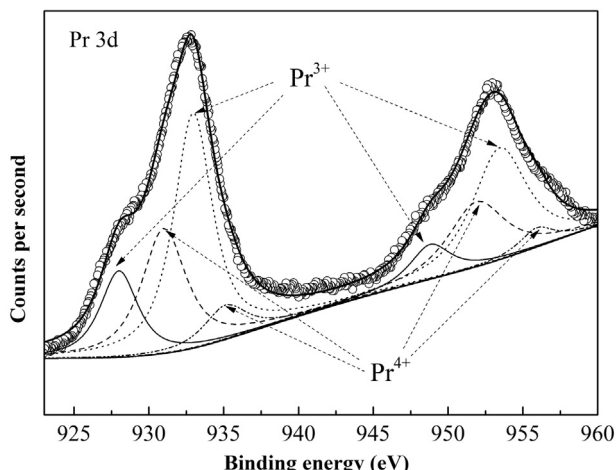


Fig. 9. XPS spectra and fitted lines of Pr 3d in the $P_{0.42}CFN$ sample.

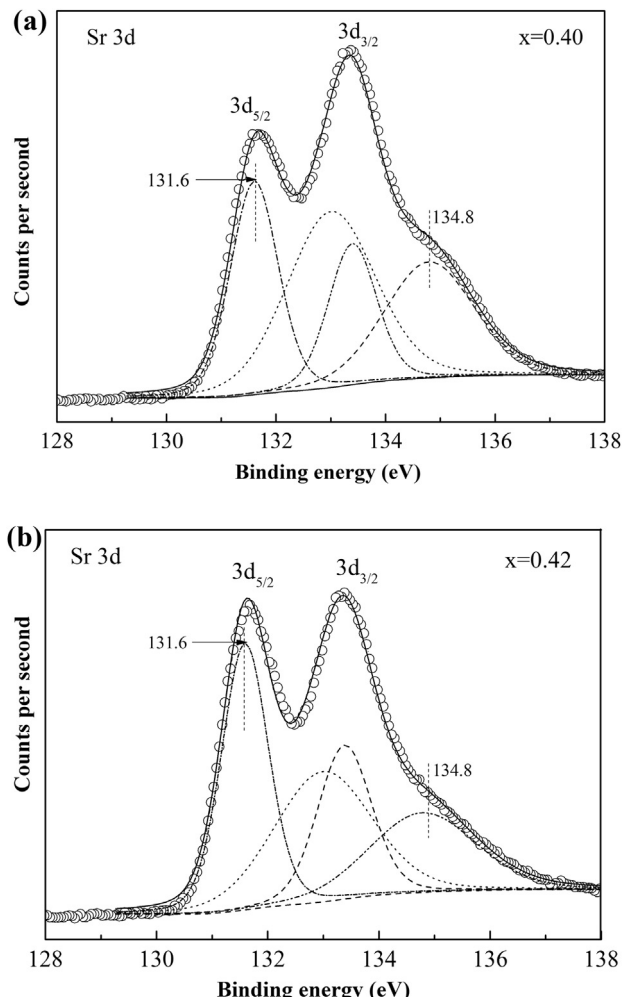


Fig. 10. XPS spectra and fitted lines of Sr 3d in the P_xSCFN sample: (a) $x = 0.40$, (b) $x = 0.42$.

temperature were owing to the more amounts of Co-enriched particles on $P_{0.42}SCFN$ anode surface than that on $P_{0.40}SCFN$, as shown in Fig. 6(c) and (d). This also proved that the nano-sized Co-enriched particles improved the reaction activity on the anode side.

Fig. 11(b) shows the fitted core-level spectrum results of Fe 2p for the $P_{0.42}SCFN$ sample. The splitting in the Fe 2p XPS spectra showed a doublet of $2\text{p}_{3/2}$ and $2\text{p}_{1/2}$ excitation. Cheng et al. [40] reported that the peaks near 709.3 eV can be ascribed to Fe^{2+} $2\text{p}_{3/2}$. For the species of Fe^{3+} , the peak position of Fe^{3+} $2\text{p}_{3/2}$ was found to be between 710.6 and 711.2 eV, [41,42] while the peak appeared in the range of 712–714 eV can be ascribed to Fe^{4+} [43]. Toru et al. [44] obtained the binding energies of Fe_2O_3 $2\text{p}_{3/2}$ and $2\text{p}_{1/2}$ at 711.0 and 724.6 eV, respectively. The peak with respect to Fe_2O_3 was found to associate the satellite peak, which is located at the position approximately 8 eV higher than the main Fe 2p_{3/2} peak. Therefore, the main peaks of binding energy at 709.3, 710.8 and 713.4 eV, as shown in Fig. 9(b), are assigned to Fe^{2+} $2\text{p}_{3/2}$, Fe^{3+} $2\text{p}_{3/2}$ and Fe^{4+} $2\text{p}_{3/2}$, respectively [43,45,46]. The satellite peak around 718.5 eV should be assigned to the Fe^{3+} species. The binding energy of Fe 2p for $P_{0.42}SCFN$ is different with those of Fe^{2+} 2p, Fe^{3+} 2p and Fe^{4+} 2p, indicating that Fe in PSCFN is in a mixed valence state. In the ABO_3 perovskite P_xSCFN oxides, Pr and La occupy the A-site; Co, Fe and Nb occupy the B-site. The doping of $\text{Pr}^{3+}/4^+$ in A-site and Nb^{5+} in B-site and the forming of oxygen vacancies resulted in the increasing of the valence of P_xSCFN oxides. Therefore, based on the electroneutrality principle, Co^{4+} and Fe^{4+} should be decreased

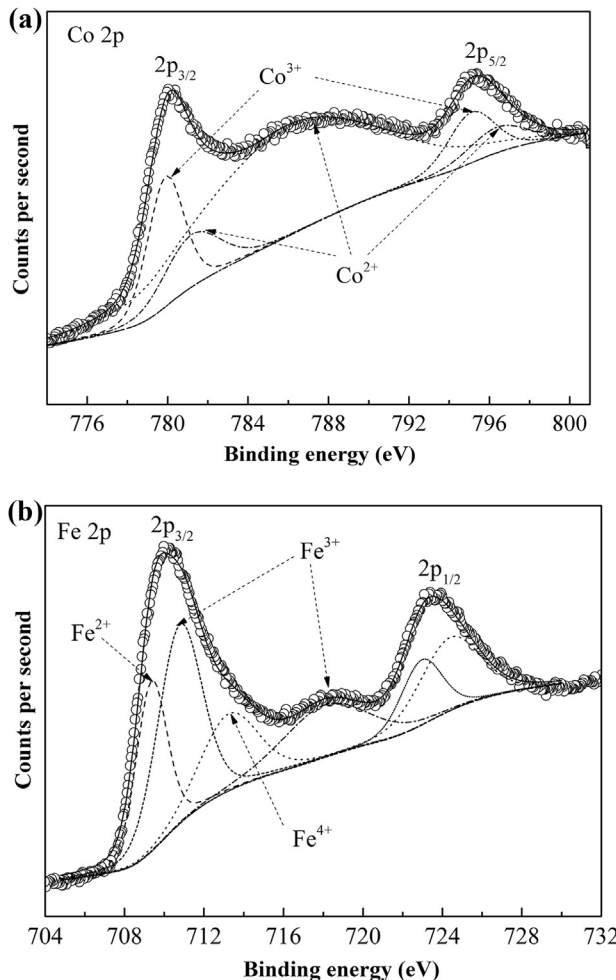
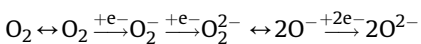


Fig. 11. XPS spectra and fitted lines of (a) Co 2p and (b) Fe 2p in the P_{0.42}SCFN sample.

to Co²⁺/Co³⁺ and Fe²⁺/Fe³⁺. From Fig. 11(a) and (b), all of the Co⁴⁺ were reduced to Co²⁺ and Co³⁺; however, Fe⁴⁺ was coexisted with Fe²⁺ and Fe³⁺. It indicated that the Co⁴⁺ was more easily reduced to Co³⁺/Co²⁺ than Fe⁴⁺, the similar phenomenon was also observed by Tai et al. [47].

Fig. 12 shows the O 1s core-level XPS spectrum of the P_{0.40}SCFN and P_{0.42}SCFN samples. The O 1s peaks at 528.5 and 529.2 eV of P_{0.40}SCFN should be attributed to the surface lattice oxygen of the perovskite structure, as shown in Fig. 12(a) [32]. In Fig. 12(b), the peak shifted toward the lower binding energy for P_{0.42}SCFN of 528.2 eV, which probably arises from a difference in the molecular environment surrounding the O atom. The characteristic peak at 531.2 eV may be ascribed to the carbonate species (CO₃²⁻) [22], which further identify the formation of SrCO₃ and adsorbed oxygen species. The adsorbed oxygen species may contain O₂⁻, O₂²⁻, O⁻ and so on. A series of transformations could happen on the surface of oxide following the general scheme [48]:



where the underline refers to the chemisorbed or surface species. From this scheme, different species of adsorbed oxygen are formed, gradually enriched with electrons until the state of O²⁻ is reached, which may be considered as lattice oxygen incorporated into the uppermost surface layer of the solid. Comparing to Fig. 12 (a) and (b), the peak at ~531 eV of P_{0.40}SCFN sample was much larger

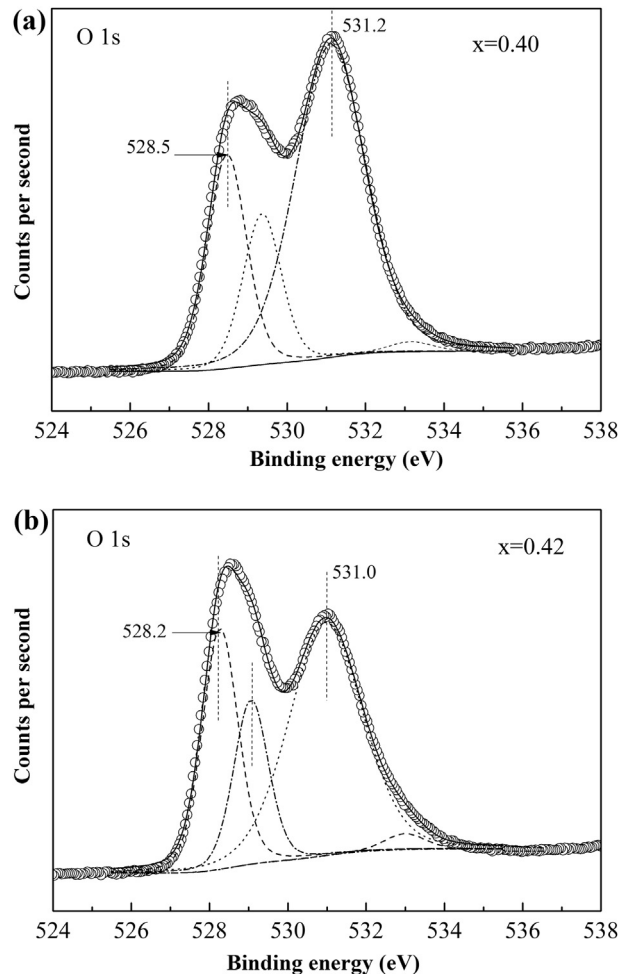


Fig. 12. XPS spectra and fitted lines of O 1s in the P_xSCFN sample: (a) x = 0.40, (b) x = 0.42.

than that of P_{0.42}SCFN sample, which indicates that there are more adsorbed oxygen species on the surface of P_{0.40}SCFN oxide. This result is consistent with the XPS spectra of Sr shown in Fig. 12(a) and (b). The absorbed oxygen on the outmost surface in transition metal oxides should be also related to the amount of oxygen deficiency [35]. Therefore, the oxygen deficiency decrease may be a compensation of valence with increasing A-site Pr element contents, which could enhance the cation concentration in the P_xSCFN oxides.

4. Conclusions

In this study, the effect of Pr element contents on the cell performance of the P_xSCFN symmetrical electrode SOFC was investigated in details and the following results were obtained.

- (1) The maximum power densities of 0.653, 0.859, 1.133 and 0.972 W cm⁻² at 900 °C for P_{0.38}SCFN, P_{0.40}SCFN, P_{0.42}SCFN and P_{0.44}SCFN based symmetrical electrode SOFC, respectively, were obtained.
- (2) The cell performance was found to be improved obviously by elevating the operation temperature for all tested P_xSCFN symmetrical electrode SOFC and by increasing Pr element content when x ≤ 0.42. However, when further increased x to 0.44, the cell performance slightly became worse at each

- temperature. Furthermore, for a single cell with $P_{0.42}SCFN$ based symmetrical electrode shows an average slow degradation rate of 0.5 mV h^{-1} during 100 h stability test, indicating that the symmetrical SOFC with PSCFN as electrode has the acceptable stabilization.
- (3) The nano-sized Co-enriched particles formed on the anode surface, improved the catalytic activities of anode side reactions.
 - (4) The grain size on the electrode was found to be decreased by increasing Pr concentrations. The finer grain size could produce larger TPB areas for the electrochemical reaction and provide larger contact area between LSGM electrolyte and P_xSCFN electrode, which contributed to the improvement of the power density P_xSCFN symmetrical electrode SOFC.
 - (5) XPS analysis indicated that $\text{Pr}^{3+}/\text{Pr}^{4+}$, $\text{Co}^{2+}/\text{Co}^{3+}$ and $\text{Fe}^{2+}/\text{Fe}^{3+}/\text{Fe}^{4+}$, which relate to catalytic activity, coexisted in PSCFN sample while the content of Sr^{2+} species on the surface decreased to some extent in the case of A-site Pr element slight excess, which could result in the promoting of the catalytic properties of PSCFN material.

Acknowledgments

This study was supported by Aomori City Government. P. Zhang gratefully acknowledges the scholarship from the State Scholarship Fund of China Scholarship Council (2012) and Deni S. Khaerudini gratefully acknowledges the scholarship from the Ministry of Education, Culture, Sports, Science and Technology (MEXT) of Japan. The authors also thank Dr Seiji Kakuta at Aomori Prefectural Industrial Technology Research Center for their technical support on experiments.

References

- [1] Q.M. Nguyen, T. Takahashi, Elsevier Science Ltd. (1995).
- [2] S.C. Singhal, K. Kendall, Elsevier Science Ltd. (2003).
- [3] A. Choudhury, H. Chandra, A. Arora, *Renew. Sust. Energ. Rev.* 20 (2013) 430–442.
- [4] D.M. Bastidas, S. Tao, J.T.S. Irvine, *J. Mater. Chem.* 16 (2006) 1603–1605.
- [5] J.C. Ruiz-Morales, J. Canales-Vázquez, J. Peña-Martínez, D.M. López, P. Núñez, *Electrochim. Acta* 52 (2006) 278–284.
- [6] X. Zhu, Z. Lü, B. Wei, X. Huang, Y. Zhang, W. Su, *J. Power Sources* 196 (2011) 729–733.
- [7] Q. Liu, X. Dong, G. Xiao, F. Zhao, F. Chen, *Adv. Mater.* 22 (2010) 5478–5482.
- [8] R. Martínez-Coronado, A. Aguadero, D. Pérez-Coll, L. Troncoso, J.A. Alonso, M.T. Fernández-Díaz, *Int. J. Hydrogen Energy* 37 (2012) 18310–18318.
- [9] M. Chen, S. Paulson, V. Thangadurai, V. Birss, *J. Power Sources* 236 (2013) 68–79.
- [10] P. Zhang, G. Guan, D.S. Khaerudini, X. Hao, M. Han, Y. Kasai, K. Sasagawa, A. Abdula, *J. Power Sources* 248 (2014) 163–171.
- [11] S. Park, J.M. Vohs, R.J. Gorte, *Nature* 404 (2000) 265–267.
- [12] S. Tao, J.T.S. Irvine, *J. Electrochem. Soc.* 151 (2004) A497–A503.
- [13] R. Martínez-Coronado, J.A. Alonso, A. Aguadero, M.T. Fernández-Díaz, *Int. J. Hydrogen Energy* 39 (2014) 4067–4073.
- [14] H. Lv, H. Tu, B. Zhao, Y. Wu, K. Hu, *Solid State Ionics* 177 (2007) 3467–3472.
- [15] C. Zhao, R. Liu, S. Wang, Z. Wang, J. Qian, T. Wen, *J. Power Sources* 192 (2009) 552–555.
- [16] M.J. Jorgensen, M. Mogensen, *J. Electrochem. Soc. A* 148 (5) (2001) A433–A442.
- [17] W. Zhou, R. Ran, Z. Shao, W. Zhuang, J. Jia, H. Gu, *Acta Mater.* 56 (2008) 2687–2698.
- [18] B. Jaffe, W.R. Cook, H. Jaffe, *Piezoelectric ceramics*, New York, Academic Press, 1971.
- [19] H. Sumi, T. Yamaguchi, K. Hamamoto, T. Suzuki, Y. Fujishiro, *J. Power Sources* 226 (2013) 354–358.
- [20] C. Yang, Z. Yang, C. Jin, G. Xiao, F. Chen, M. Han, *Adv. Mater.* 24 (2012) 1439–1443.
- [21] R. Scurtu, S. Somacescu, J.M. Calderon-Moreno, D. Culita, I. Bulimestr, N. Popa, *J. Solid State Chem.* 210 (2014) 53–59.
- [22] B. Liu, Y. Zhang, L. Tang, *Int. J. Hydrogen Energy* 34 (2009) 435–439.
- [23] Y. Liu, J. Chen, F. Wang, B. Chi, J. Pu, L. Jian, *Int. J. Hydrogen Energy* 39 (7) (2014) 3404–3411.
- [24] X. Pan, Z. Wang, B. He, S. Wang, X. Wu, C. Xia, *Int. J. Hydrogen Energy* 38 (2013) 4108–4115.
- [25] C. Abate, V. Esposito, K. Duncan, J.C. Nino, D.M. Gattia, E.D. Wachsman, *J. Am. Ceram. Soc.* 93 (7) (2010) 1970–1977.
- [26] T. Ishihara, T. Kudo, H. Matsuda, Y. Takita, *J. Electrochem. Soc.* 142 (5) (1995) 1519–1524.
- [27] F. Jin, Y. Shen, R. Wang, T. He, *J. Power Sources* 234 (2013) 244–251.
- [28] E.V. Tsipis, V.V. Kharton, *J. Solid State Electrochem.* 12 (2008) 1367–1391.
- [29] H. He, H.X. Dai, C.T. Au, *Catal. Today* 90 (2004) 245–254.
- [30] A.A. Yaremchenko, S.G. Patrício, J.R. Frade, *J. Power Sources* 245 (2014) 557–569.
- [31] R. Polini, A. Falsetti, E. Traversa, O. Schäf, P. Knauth, *J. Eur. Ceram. Soc.* 27 (2007) 4291–4296.
- [32] P.A.W. van der Heide, *Surf. Interface Anal.* 33 (2002) 414–425.
- [33] J.C. Dupin, D. Gonbeau, P. Vinatier, A. Levasseur, *Phys. Chem. Chem. Phys.* 2 (2000) 1319–1324.
- [34] Q. Wu, M. Liu, W. Jaegermann, *Mater. Lett.* 59 (2005) 1480–1483.
- [35] Y. Yin, M. Xiong, N. Yang, Z. Tong, Y. Guo, Z. Ma, *Int. J. Hydrogen Energy* 36 (2011) 3989–3996.
- [36] L.F. Liotta, G. Di Carlo, G. Pantaleo, A.M. Venezia, G. Deganello, *Appl. Catal. B Environ.* 66 (2006) 217–227.
- [37] M. Oku, Y. Sato, *Appl. Surf. Sci.* 55 (1992) 37–41.
- [38] A.S. Harvey, F.J. Litterst, Z. Yang, J.L.M. Rupp, A. Infortuna, L.J. Gauckler, *Phys. Chem. Chem. Phys.* 11 (2009) 3090–3098.
- [39] Z. Yang, A.S. Harvey, A. Infortuna, J. Schoonman, L.J. Gauckler, *J. Solid State Electrochem.* 15 (2) (2011) 277–284.
- [40] W. Cheng, X. Ma, *J. Phys. Conf. Ser.* 152 (2009) 012039.
- [41] S.J. Roosendaal, B. v. Asselen, J.W. Elsenaar, A.M. Vredenberg, F.H.P.M. Habraken, *Surf. Sci. Rep.* 442 (1999) 329–337.
- [42] P.C.J. Graat, M.A.J. Somers, *Appl. Surf. Sci.* 100/101 (1996) 36–40.
- [43] Y. Bu, Q. Zhong, D. Xu, W. Tan, *J. Alloys Compd.* 578 (2013) 60–66.
- [44] T. Yamashita, P. Hayes, *Appl. Surf. Sci.* 254 (2008) 2441–2449.
- [45] X. Zhu, Q. Zhong, D. Xu, H. Yan, W. Tan, *J. Alloys Compd.* 555 (2013) 169–175.
- [46] G. Xiao, Q. Liu, S. Wang, V.G. Komvokis, M.D. Amiridis, A. Heyden, *J. Power Sources* 202 (2012) 63–69.
- [47] L. Tai, M.M. Nasrallah, H.U. Anderson, D.M. Sparlin, S.R. Sehlin, *Solid State Ionics* 76 (1995) 259–271.
- [48] N.A. Merino, B.P. Barbero, P. Eloy, L.E. Cadús, *Appl. Surf. Sci.* 253 (2006) 1489–1493.